

# Spatially coherent high-order harmonics generated at optimal high gas pressure with high-intensity one- or two-color laser pulses

Cheng Jin<sup>1,\*</sup> and C. D. Lin<sup>2</sup><sup>1</sup>*Department of Applied Physics, Nanjing University of Science and Technology, Nanjing, Jiangsu 210094, People's Republic of China*<sup>2</sup>*J. R. Macdonald Laboratory, Department of Physics, Kansas State University, Manhattan, Kansas 66506, USA*

(Received 9 August 2016; published 4 October 2016)

We investigate the gas-pressure dependence of macroscopic harmonic spectra generated in a high-ionization medium using intense 800-nm laser pulses. The harmonics obtained at the optimal pressure show good spatial coherence with small divergence (less than 2 mrad) in the far field. By analyzing the evolution of the laser's electric field as it propagates, we find that dynamic phase matching conditions are fulfilled in the second half of the gas cell and that harmonic yields do not depend on the position of the gas cell with respect to the focusing position. We also demonstrate that harmonic yields at the optimal pressure can be further enhanced by increasing input laser energy or by adding a few percent of second or third harmonic to the fundamental.

DOI: [10.1103/PhysRevA.94.043804](https://doi.org/10.1103/PhysRevA.94.043804)

## I. INTRODUCTION

High harmonics generated by an intense laser pulse interacting with atomic gas media is an important technique for providing useful bright and coherent tabletop light sources from the extreme ultraviolet (XUV) to x rays in the form of single attosecond pulses or pulse trains [1–4]. They have served as essential tools in many research areas like femtosecond spectroscopy [5], attosecond physics [6], seeded free electron lasers [7], and high-resolution imaging [8]. However, applications of high-order harmonic generation (HHG) have been limited by the low conversion efficiency. To increase efficiency, one can either create favorable phase-matching conditions in a nonlinear medium [9,10] or modify subcycle optical waveforms to enhance single-atom yields [11–18].

Previously we have examined different schemes of waveform synthesis of multicolor sinusoidal laser pulses such as (i) combining two- or three-color fields without restriction on their relative intensities [19], (ii) combining a strong midinfrared laser with optimized wavelength and a few percent of its third harmonic to efficiently extend the harmonic plateau to the keV region [20], and (iii) adding a strong 800-nm pulse and a relatively weak midinfrared laser to enhance harmonic yields in the water-window region [21]. Optimized waveforms thus obtained are capable of enhancing the generated harmonics by one to two orders. The schemes above were obtained at the low ionization level (a few percent) and at low gas pressure to prevent detrimental plasma dispersion due to excessive free electrons in the gas medium.

High harmonics have been generated under high gas pressure in a gas cell [22] or in a hollow-core waveguide [10,23] using long-wavelength lasers. HHG experiments have also been carried out at high laser intensity and high gas pressure with 750-nm Ti:sapphire lasers [24]. In spite of high free electron density (ionization level at several tens of percent) in the gas medium, dynamic phase matching appears to have been achieved since intense high harmonics have been observed.

The main goal of this paper is to analyze how dynamic phase matching actually works at optimal pressure. We will first investigate the pressure dependence of macroscopic HHG spectra of Ne atoms exposed to a high-intensity 800-nm laser pulse where we can compare our simulation with a recent experiment reported by Zhao *et al.* [24]. We will then extend the analysis to two-color fields.

To describe experimentally measured high harmonics, we first calculate harmonic amplitude and phase from single atoms and then carry out macroscopic propagation in the gas medium. The single-atom response is calculated using the quantitative rescattering (QRS) model [25], and macroscopic propagation for both high harmonics and the driving laser field is obtained by solving three-dimensional Maxwell's equations [26]. The latter procedure has been applied to study plasma effect in high-harmonic generation in previous investigations also [27–31].

## II. HIGH HARMONICS WITH ONE-COLOR LASER PULSE

We show the simulated macroscopic HHG spectra of Ne atoms by varying the gas pressure from 50 to 600 Torr in Fig. 1(a). In the simulation, we choose an 800-nm laser with a FWHM duration of 8 fs (3 optical cycles). Laser beam waist  $w_0$  is 25  $\mu\text{m}$ , and peak intensity at the focus is  $10 \times 10^{14}$  W/cm<sup>2</sup>. Ionization probability at the end of laser pulse is about 25%, calculated by the modified Ammosov-Delone-Krainov (ADK) tunneling ionization model [32] to incorporate the modification in the over-the-barrier ionization regime. The gas cell is assumed to have uniform density distribution. Its length is 1 mm, and it is placed at the laser focus. From Fig. 1(a), we can see that with the increase of gas pressure the harmonic cutoff energy is gradually decreased and harmonic yields in the plateau are progressively increased. The balance between harmonic yield and plateau spectral range is best reached when the gas pressure is 300 Torr, which is taken as the optimal pressure. The dependence of the harmonic spectra on the gas pressure is about the same as in the experiment reported by Zhao *et al.* [24]. In Table I we compare the cutoff energy versus gas pressure between our simulation and the experiment. Quite good agreement can be seen even though there is a 5–10 eV difference roughly at each pressure. In Zhao *et al.* [24], the

\*Corresponding author: [cjin@njust.edu.cn](mailto:cjin@njust.edu.cn)

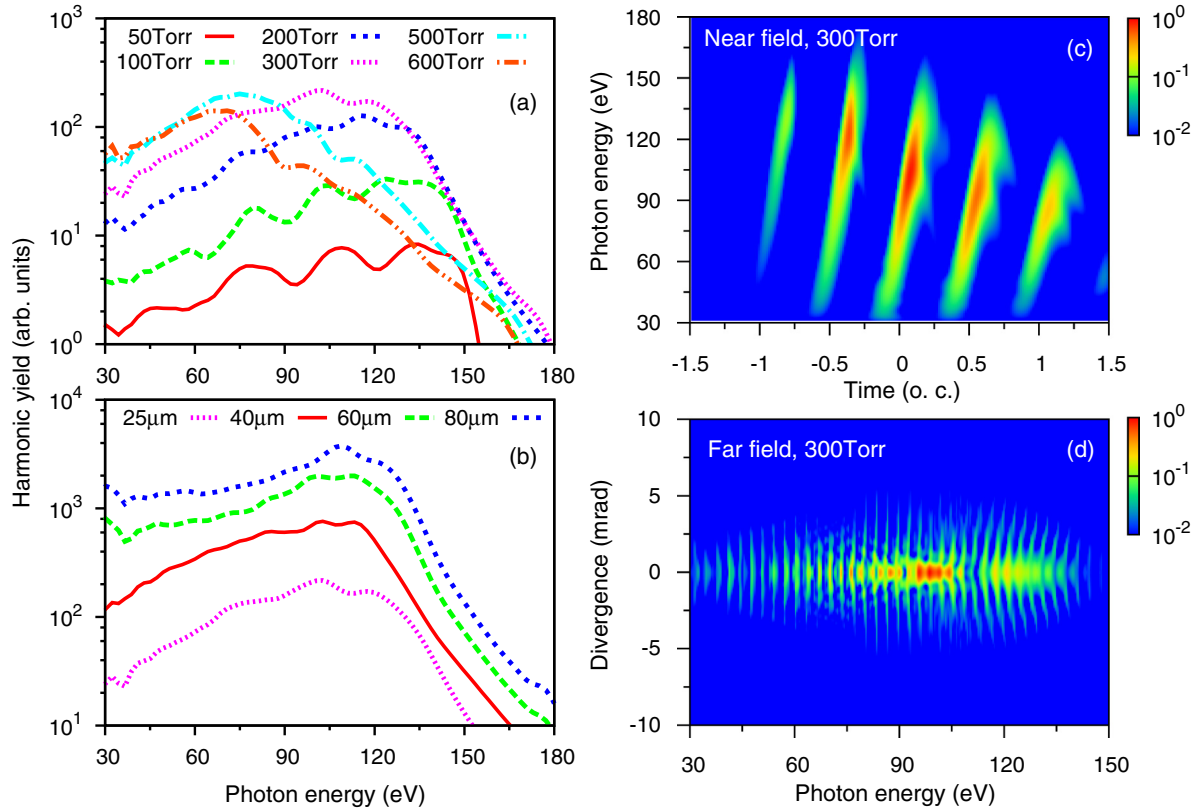


FIG. 1. HHG spectra generated in high-pressure neon gas with high-intensity 800-nm laser pulses. (a) Harmonic yields vs gas pressure. Optimal pressure for the best harmonic yields is found at 300 Torr. (b) Further increase of harmonic yield at constant peak intensity and 300 Torr pressure as the beam waist is increased, by the increase of pulse energy. (c) Time-frequency analysis of harmonic emission showing “short”-trajectory harmonics that lead to (d) low-divergence harmonics in the far field for high harmonics in (a) at 300 Torr. See text for other laser parameters.

polarization gating method was used for the generation of the harmonics. This is roughly equivalent to a single-optical-cycle, linearly polarized driving laser, while our simulations were carried out with three-cycle laser pulses. In addition, precise calibration of the gas pressure in the generation region is very difficult. These facts may explain the small discrepancy seen in the Table I.

We next analyze the harmonics generated at 300 Torr. Figure 1(c) shows the time-frequency analysis of the harmonics at the exit plane (near field) where harmonics have been integrated over the plane perpendicular to the propagation direction [33]. Note that only “short”-trajectory emissions are present and there are three major emission bursts at about  $-0.5, 0,$  and  $0.5$  optical cycles (o.c.), corresponding to electron release occurring at  $-1.0, -0.5,$  and  $0$  o.c., i.e., these harmonics are mostly emitted at the leading edge of the laser pulse. It is well known that only short-trajectory emission can survive macroscopic propagation if the laser is focused before

a gas jet [34–36]. In our case, the gas cell is located at the laser focus. We have found that focusing position is no longer essential since the laser pulse has been greatly defocused by the plasma. The short-trajectory emissions in the near field would lead to small-divergent harmonic emission in the far field, as shown in Fig. 1(d). These results clearly demonstrate that bright high harmonics up to 120 eV with divergence less than about 2 mrad are generated at high laser intensity of  $10 \times 10^{14}$  W/cm<sup>2</sup> and high gas pressure of 300 Torr. Further increase of gas pressure would reduce the intensity of the harmonics and the cutoff energy. Note that the cutoff energy based on the single atom response is about 210 eV, but Fig. 1(d) shows that after propagation the cutoff is about 140 eV. Figure 1(c) shows that higher energy harmonics can be generated at the leading edge of the pulse, but at the trailing edge only lower harmonics are generated. The origin of this difference owes to the dynamic phase matching driven by the time evolving plasma [37].

How do we understand the pressure dependence obtained from the simulation shown in Fig. 1? We examine the electric fields of the driving laser (in a reference frame moving at the speed of light) at three positions:  $z = -0.5, 0,$  and  $0.5$  mm, i.e., at the entrance, middle point, and exit plane of the gas cell, respectively, for three different gas pressures in Figs. 2(a)–2(c), at the off-axis radial position of one-third of the laser beam waist. These figures show two important features.

TABLE I. Comparison of harmonic cutoff energy with gas pressure between experiment [24] and simulation.

Gas pressure	50 Torr	100 Torr	250 Torr	500 Torr	600 Torr
Zhao <i>et al.</i> [24]	140 eV	125 eV	100 eV		
This work	145 eV	135 eV	110 eV	80 eV	70 eV

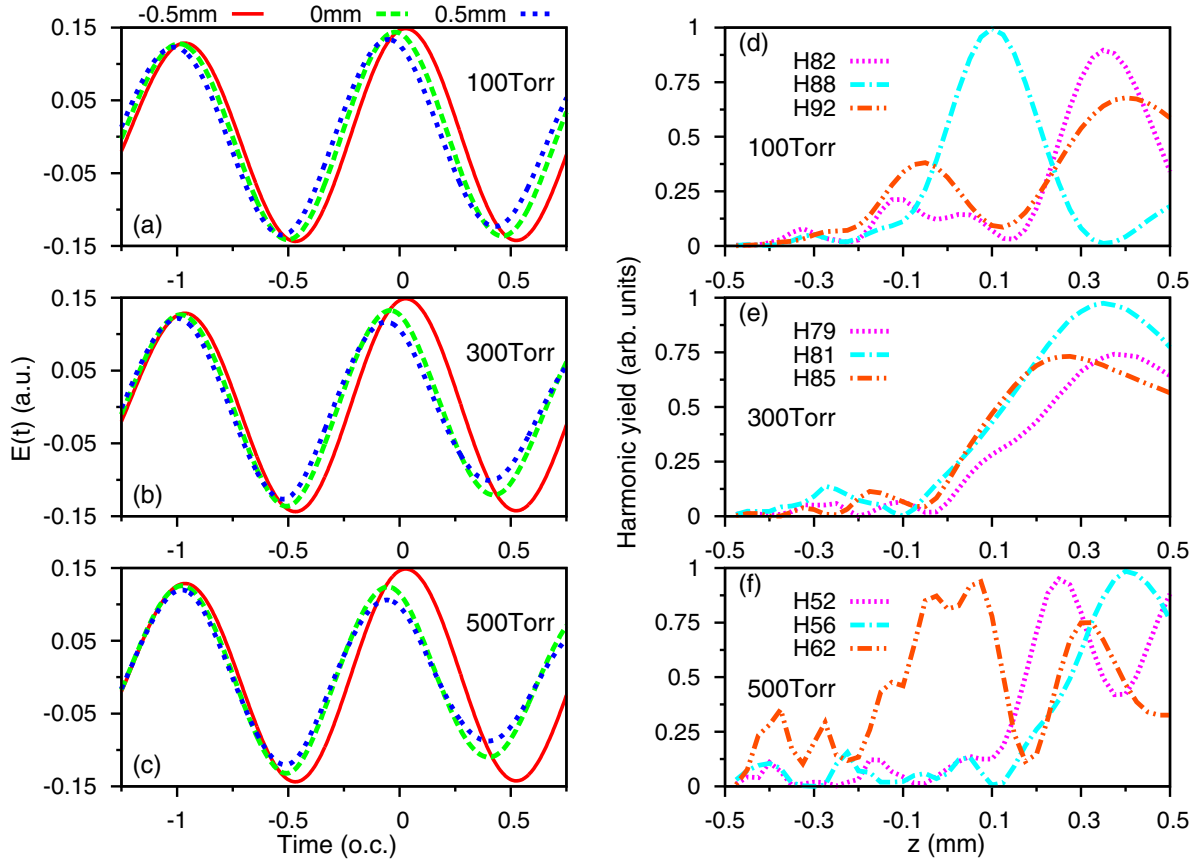


FIG. 2. (a)–(c) Off-axis (at  $r = w_0/3$ , where  $w_0 = 25 \mu\text{m}$ ) electric fields of an 800-nm laser beam at three gas pressures: 100, 300, and 500 Torr. The electric fields are shown at the entrance ( $-0.5 \text{ mm}$ ), center ( $0.0 \text{ mm}$ ), and exit ( $0.5 \text{ mm}$ ) of the gas cell (o.c. stands for optical cycle). (d)–(f) Evolution of selected harmonics at  $r = w_0/3$  with the propagation distance  $z$ , for three pressures and harmonic orders as indicated.

First, compared to the field at the entrance, the fields at the middle and at the exit are reduced. The reduction is due to the free electrons in the medium and more reduction with higher pressure. This explains why the cutoff energy shifts to lower harmonics with increasing pressure. Second, the field change is larger in the first half of the gas cell ( $z = -0.5$  to  $0 \text{ mm}$ ) than in the second half ( $z = 0$  to  $0.5 \text{ mm}$ ). In the first half, the field is still large and the ionization rate is high. The rapid change of dispersion results in a large phase mismatch and thus harmonics are unable to grow as they propagate. In the second half, the field is already weakened and it does not change much (difference between dashed green and dotted blue lines in the figures) to result in good phase matching and to allow harmonics to grow. This is confirmed quantitatively by the simulations, as shown in Figs. 2(d)–2(f). This analysis explains how phase matching is achieved for HHG under the high-intensity, high-gas-pressure condition, which is different from the low-pressure regime.

Figure 2(e) demonstrates that harmonic orders 79 (H79), 81, and 85 grow steadily from  $z = 0$  to  $0.5 \text{ mm}$  for the optimal gas pressure of 300 Torr. In the following, we show how this can be explained by the phase-matching condition. These harmonics, at photon energies around 125 eV, are emitted at about  $-0.5 \text{ o.c.}$ , as can be seen in Fig. 1(c), due to short-trajectory electrons ionized around  $-1.0 \text{ o.c.}$ , see Fig. 2(b). They do not have contributions from other optical

cycles. Because of laser field reshaping, the peak fields near  $-1.0 \text{ o.c.}$  are only slightly shifted at  $z = 0$  and  $0.5 \text{ mm}$  from the input one at  $z = -0.5 \text{ mm}$ . For each harmonic, this results in a phase mismatch [38]

$$\Delta k \approx [(q - 1)\omega_0 \Delta t - \alpha_i \Delta I] / \Delta z, \quad (1)$$

where  $q$  is the harmonic order and the second term is due to the change of dipole phase with laser intensity. For short-trajectory emissions,  $\alpha_i \approx 1 \times 10^{-14} \text{ rad cm}^2/\text{W}$  [39], and  $\Delta t$  and  $\Delta I$  are the shift of the peak electric field in time and intensity variation over a propagation distance  $\Delta z$ , respectively. The latter values are listed in Table II. For  $\Delta z = 0.5 \text{ mm}$ ,  $\Delta t = -0.031 \text{ fs}$ , and  $\Delta I = -0.45 \times 10^{14} \text{ W/cm}^2$ , the coherence length  $L_{\text{coh}} = \pi / |\Delta k|$ , with  $\Delta k$  calculated from Eq. (1) is about  $0.3 \text{ mm}$  for H79. This is consistent with the coherence length observed for H79 in Fig. 2(e) where the harmonic yield grows steadily from  $z = 0 \text{ mm}$  to a maximum at  $z = 0.35 \text{ mm}$ . For H81 and H85 they behave similarly; these harmonics remain near the peak values at the exit plane of  $z = 0.5 \text{ mm}$ . Such analysis illustrates how good phase matching for these high harmonics is achieved at 300 Torr. Note that the two terms in Eq. (1) are not entirely independent for laser propagation in the gas medium.

For pressure at 100 Torr, the larger mismatch of electric fields between  $z = 0$  and  $0.5 \text{ mm}$  [see Fig. 2(a)] gives a smaller coherence length for the three harmonics shown in Fig. 2(d)

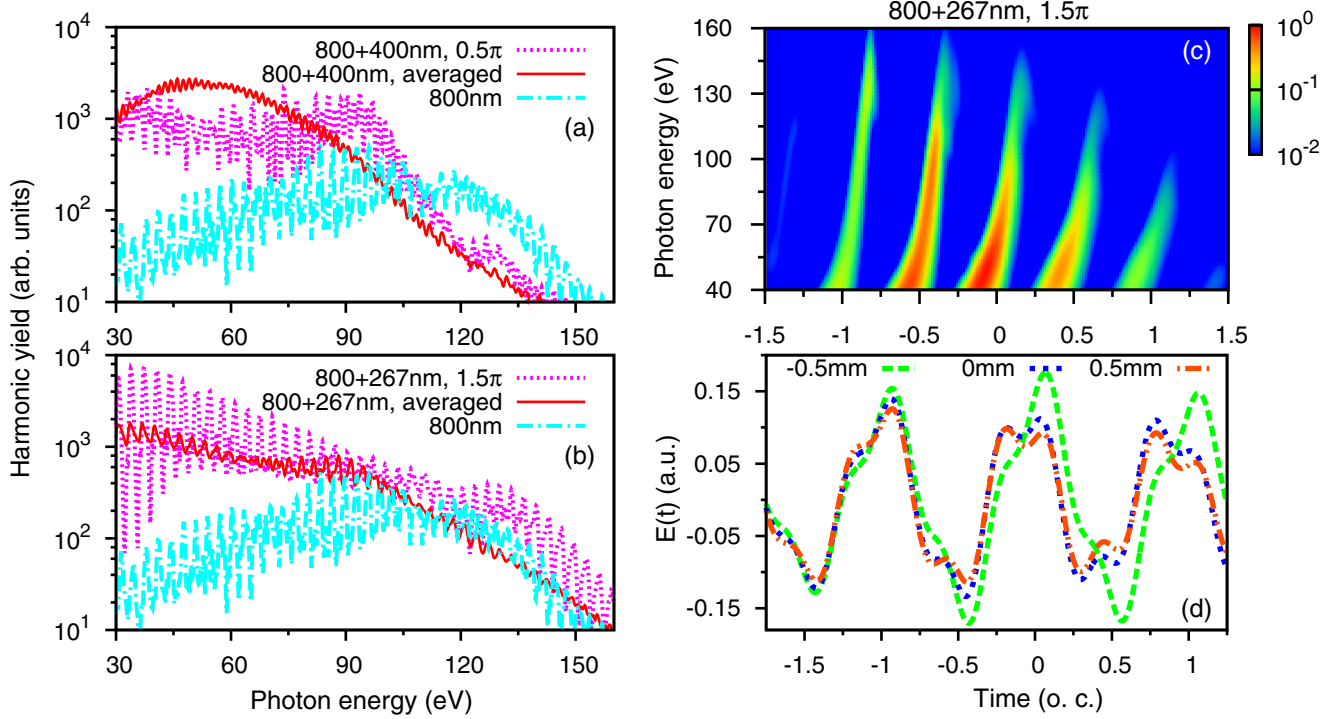


FIG. 3. Simulated macroscopic HHG spectra of Ne atoms by two-color laser pulses at the optimal pressure of 300 Torr: (a) 800 + 400 nm, and (b) 800 + 267 nm, with fixed or random relative phase between the two colors. See text for other laser parameters. Results of a single 800-nm laser pulse are plotted for comparison. (c) Time-frequency representation of harmonic emission in the near field, and (d) off-axis electric fields (at  $r = w_0/3$ ) at the entrance ( $-0.5$  mm), center (0 mm), and exit (0.5 mm) of the gas cell for 800 + 267 nm laser with relative phase of  $1.5\pi$ .

(measured by the length  $\delta z$  where the harmonics are building up monotonically before they fall again). For instance, the calculated coherence length  $L_{\text{coh}}$  for H82 is about 0.14 mm by using Eq. (1), which agrees with the growth length from  $z = 0.15$  mm to a maximum at  $z = 0.3$  mm in Fig. 2(d). At 500 Torr, we have checked that harmonics are generated from multiple emission bursts. The selected harmonics in Fig. 2(f) are the result of intercycle interference and do not show fixed coherence length as they propagate in the medium.

From Table II, phase mismatch from the intrinsic single-atom phase is much smaller than the mismatch arising from the difference in the electric fields. Thus the single-atom phase term can be ignored if only short-trajectory emissions are present. We can then conclude that at the optimal pressure of 300 Torr, high harmonics are efficiently generated when

TABLE II. The instant ( $t_p$  around  $-1$  o.c.) and the strength ( $E_p$ ) of the peak electric field of the laser pulse in Fig. 2(b) at propagation positions:  $z = 0$  and 0.5 mm. The phase mismatch calculated according to Eq. (1) is also shown.

$z = 0$ mm		$z = 0.5$ mm	
$t_p$ (fs)	$E_p$ (a.u.)	$t_p$ (fs)	$E_p$ (a.u.)
-2.625	0.1266	-2.656	0.1214
Phase mismatch $\Delta k$ (rad/mm)			
$(q - 1)\omega_0 \Delta t / \Delta z$		$-\alpha_i \Delta I / \Delta z$	
-11.39 ( $q = 79$ )		0.91 (short)	

the mismatch of electric fields over several optical cycles at different  $z$  is minimized. Therefore, optimal harmonics are generated at the pressure where dynamic phase matching is fulfilled and the driving laser field remains relatively high even with the presence of electrons. (The peak intensity from Table II is about  $5.60 \times 10^{14}$  W/cm<sup>2</sup> at  $z = 0$  mm, compared to  $5.85 \times 10^{14}$  W/cm<sup>2</sup> at the entrance at the same radial distance of  $r = w_0/3$ .)

The above analysis explains how dynamic phase matching is accomplished under the high-pressure and high-ionization condition. When laser parameters and focusing conditions are changed, the optimal pressure may change. To further increase harmonic yields at the same optimal pressure, one way is to increase the input laser energy while maintaining the same peak intensity. This is easily achieved by adjusting the focal length of the focusing mirror to increase the beam waist. In Fig. 1(b), we show HHG spectra obtained with beam waists at 40, 60, and 80  $\mu\text{m}$ , to compare with the tightly focused beam of 25  $\mu\text{m}$ . Gas pressure is the same 300 Torr while other parameters are the same as those in Fig. 1(a). With the increase of beam waist, harmonic yields increase monotonically, roughly proportional to the square of the beam waist, with the cutoff energy remaining stable at about 120 eV. We have checked that the divergence of the harmonics in the far field also stay about the same as the tight focusing condition before. Of course this would require quadratic increase of the beam energy of the driving laser. Note that shaping the beam profile is another possible way to increase harmonic yields in which poor phase matching in the initial stage of propagation could be improved [40].

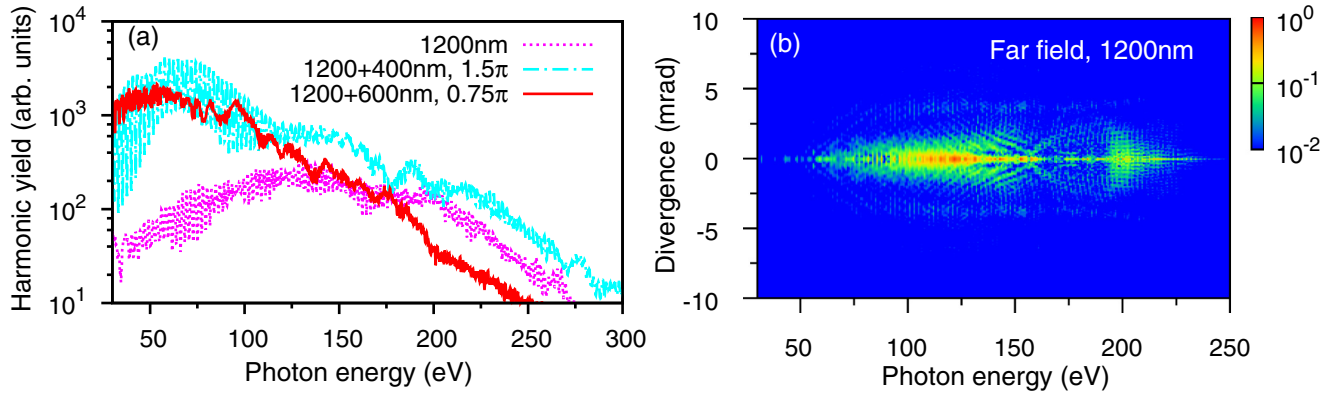


FIG. 4. (a) Comparison of simulated macroscopic HHG spectra using 1200-nm and two-color (1200 + 600 nm or 1200 + 400 nm) laser pulses at the optimal pressure of 500 Torr. See text for other laser parameters. (b) Harmonic profile in the far field generated by a single-color 1200-nm laser.

### III. HIGH HARMONICS WITH TWO-COLOR LASER PULSE

We then check if the same optimized gas pressure also works for a synthesized wave where a second (or third) harmonic with 10% (or 5%) intensity of the 800-nm laser is added to the fundamental driving laser. The answer is yes. In Figs. 3(a) and 3(b), we show the harmonic yields obtained where the relative phase of the second (or third) harmonic with respect to the 800-nm one has been optimized, and when the relative phase is random, respectively. Beam waist and pulse duration of the second (or third) harmonic are assumed to be identical to the 800-nm one. Figure 3(a) shows that high harmonics from 30 to 100 eV are enhanced by a factor of 5–10 at the optimized relative phase of  $0.5\pi$  found in our previous two-color waveform study [19]. Even if the relative phase is random, the averaged high-harmonic yields are still significantly enhanced from 30 to 90 eV. In Fig. 3(b), we choose the phase of  $1.5\pi$  for the third harmonic which is close to our previously obtained optimal value [19,20]. The yields of high harmonics from 30 to 160 eV are enhanced by a factor of 5–50. In Fig. 3(c), time-frequency analysis shows that only short-trajectory emissions contribute to the harmonics. We have also checked that harmonics at the far field have good spatial coherence. The evolution of off-axis electric fields shown in Fig. 3(d) indicates that electric fields in the time interval of  $-1.5$  to  $1.0$  o.c. are well overlapped for  $z = 0$  to  $0.5$  mm, i.e., in the second half of the gas cell. The two-color waveform in the leading edge of the laser pulse, especially around  $-1.0$  and  $-0.5$  o.c., maintains relatively high peak intensities. This example shows that the two-color and the single-color pulses have the same phase-matching mechanism and efficient growth of harmonics and dynamic phase matching occur in the second half of the gas cell at the optimal pressure of 300 Torr.

Finally we simulate HHG spectra with a 1200-nm laser, and with a two-color laser by adding 10% (or 5%) of its second (or third) harmonic, at the optimal pressure of 500 Torr, as shown in Fig. 4(a). The FWHM duration is 12 fs, beam waist  $w_0$  is  $30.6\ \mu\text{m}$  to ensure that the 1200-nm laser has the same Rayleigh length as the 800-nm one, and peak intensity at

focus is  $10 \times 10^{14}\ \text{W}/\text{cm}^2$ . Similar degree of enhancement of harmonic yields as shown in the 800-nm case using a two-color waveform is demonstrated in Fig. 4(a). We also show that the divergence of the harmonics in the far field for the 1200-nm laser in Fig. 4(b) is small, mostly less than 2 mrad over an energy region of 200 eV. Thus the mechanism of generating a spatially coherent HHG beam under high intensity and high pressure, for one- or two-color laser pulses, is not changed by varying the laser wavelength.

### IV. CONCLUSIONS

In summary, we examined phase-matching conditions of the generation of high-order harmonics of neon at high pressure and high incident intensity ( $10 \times 10^{14}\ \text{W}/\text{cm}^2$ ) for the 800-nm driving laser. We found that the optimal pressure for maximal harmonic yields was about 300 Torr which was consistent with the experimental value reported in Ref. [24]. We followed the change of the driving laser pulse inside the gas cell and analyzed the dynamic phase-matching mechanism for different gas pressures. To further increase the harmonics generated, we showed that one can either increase the laser power and beam waist simultaneously (to maintain high intensity) or add a few percent of a second or third harmonic of the driving 800-nm pulse. Each method can further increase harmonic yields by another tenfold, at the same 300-Torr optimal pressure. By increasing the fundamental driving laser wavelength to 1200 nm, the optimal pressure was found to be at 500 Torr. Our results show that harmonics can be efficiently generated under the high-intensity and high-pressure condition where the ionization fraction is large. Efficient generation occurs at an optimal pressure which can be identified by theoretical simulation or explored experimentally. We emphasize that the phase-matching conditions considered here are different from the low-pressure and low-ionization regime, where the laser geometry plays an important role [34–36]. The phase mismatch by plasma dispersion is mainly balanced by the phase mismatch due to the changing driving laser pulse in the propagation medium, not by the atomic dispersion solely as in the low-ionization level case [23].

## ACKNOWLEDGMENTS

C.J. was supported by Fundamental Research Funds for the Central Universities of China under Grant No. 30916011207. C.D.L. was supported by Chemical Sciences,

Geosciences and Biosciences Division, Office of Basic Energy Sciences, Office of Science, U. S. Department of Energy under Grant No. DE-FG02-86ER13491 and by U.S. Air Force Office of Scientific Research under Grant No. FA9550-14-1-0255.

- 
- [1] C. Spielmann, N. H. Burnett, S. Sartania, R. Koppitsch, M. Schnürer, C. Kan, M. Lenzner, P. Wobrauschek, and F. Krausz, *Science* **278**, 661 (1997).
- [2] E. J. Takahashi, T. Kanai, K. L. Ishikawa, Y. Nabekawa, and K. Midorikawa, *Phys. Rev. Lett.* **101**, 253901 (2008).
- [3] H. Xiong, H. Xu, Y. Fu, J. Yao, B. Zeng, W. Chu, Y. Cheng, Z. Xu, E. J. Takahashi, K. Midorikawa, X. Liu, and J. Chen, *Opt. Lett.* **34**, 1747 (2009).
- [4] M.-C. Chen, P. Arpin, T. Popmintchev, M. Gerrity, B. Zhang, M. Seaberg, D. Popmintchev, M. M. Murnane, and H. C. Kapteyn, *Phys. Rev. Lett.* **105**, 173901 (2010).
- [5] S. L. Sorensen, O. Bjornholm, I. Hjelte, T. Kihlgren, G. Ohrwall, S. Sundin, S. Svensson, S. Buil, D. Descamps, and A. L'Huillier, *J. Chem. Phys.* **112**, 8038 (2000).
- [6] F. Krausz and M. Ivanov, *Rev. Mod. Phys.* **81**, 163 (2009).
- [7] G. Lambert, T. Hara, D. Garzella, T. Tanikawa, M. Labat, B. Carre, H. Kitamura, T. Shintake, M. Bougeard, S. Inoue, Y. Tanaka, P. Salieres, H. Merdji, O. Chubar, O. Gobert, K. Tahara, and M.-E. Couprie, *Nat. Phys.* **4**, 296 (2008).
- [8] R. L. Sandberg, C. Song, P. W. Wachulak, D. A. Raymondson, A. Paul, B. Amirbekian, E. Lee, A. E. Sakdinawat, C. La-O-Vorakiat, M. C. Marconi, C. S. Menoni, M. M. Murnane, J. J. Rocca, H. C. Kapteyn, and J. Miao, *Proc. Natl. Acad. Sci. U.S.A.* **105**, 24 (2008).
- [9] V. S. Yakovlev, M. Ivanov, and F. Krausz, *Opt. Express* **15**, 15351 (2007).
- [10] T. Popmintchev, M.-C. Chen, D. Popmintchev, P. Arpin, S. Brown, S. Ališauskas, G. Andriukaitis, T. Balciunas, O. D. Mücke, A. Pugžlys, A. Baltuška, B. Shim, S. E. Schrauth, A. Gaeta, C. Hernández-García, L. Plaja, A. Becker, A. Jaron-Becker, M. M. Murnane, and H. C. Kapteyn, *Science* **336**, 1287 (2012).
- [11] S. Watanabe, K. Kondo, Y. Nabekawa, A. Sagisaka, and Y. Kobayashi, *Phys. Rev. Lett.* **73**, 2692 (1994).
- [12] I. J. Kim, C. M. Kim, H. T. Kim, G. H. Lee, Y. S. Lee, J. Y. Park, D. J. Cho, and C. H. Nam, *Phys. Rev. Lett.* **94**, 243901 (2005).
- [13] L. E. Chipperfield, J. S. Robinson, J. W. G. Tisch, and J. P. Marangos, *Phys. Rev. Lett.* **102**, 063003 (2009).
- [14] S.-W. Huang, G. Cirimi, J. Moses, K.-H. Hong, S. Bhardwaj, J. R. Birge, L.-J. Chen, E. Li, B. J. Eggleton, G. Cerullo, and F. X. Kärtner, *Nat. Photon.* **5**, 475 (2011).
- [15] P. Wei, J. Miao, Z. Zeng, C. Li, X. Ge, R. Li, and Z. Xu, *Phys. Rev. Lett.* **110**, 233903 (2013).
- [16] F. Brizuela, C. M. Heyl, P. Rudawski, D. Kroon, L. Rading, J. M. Dahlström, J. Mauritsson, P. Johnsson, C. L. Arnold, and A. L'Huillier, *Sci. Rep.* **3**, 1410 (2013).
- [17] E. J. Takahashi, P. Lan, O. D. Mücke, Y. Nabekawa, and K. Midorikawa, *Nat. Commun.* **4**, 2691 (2013).
- [18] S. Haessler, T. Balčiunas, G. Fan, G. Andriukaitis, A. Pugžlys, A. Baltuška, T. Witting, R. Squibb, A. Zair, J. W. G. Tisch, J. P. Marangos, and L. E. Chipperfield, *Phys. Rev. X* **4**, 021028 (2014).
- [19] C. Jin, G. Wang, H. Wei, A.-T. Le, and C. D. Lin, *Nat. Commun.* **5**, 4003 (2014).
- [20] C. Jin, G. Wang, A. T. Le, and C. D. Lin, *Sci. Rep.* **4**, 7067 (2014).
- [21] C. Jin, K.-H. Hong, and C. D. Lin, *Opt. Lett.* **40**, 3754 (2015).
- [22] K.-H. Hong, C.-J. Lai, J. P. Siqueira, P. Krogen, J. Moses, C.-L. Chang, G. J. Stein, L. E. Zapata, and F. X. Kärtner, *Opt. Lett.* **39**, 3145 (2014).
- [23] T. Popmintchev, M.-C. Chen, A. Bahabad, M. Gerrity, P. Sidorenko, O. Cohen, I. P. Christov, M. M. Murnane, and H. C. Kapteyn, *Proc. Natl. Acad. Sci. USA* **106**, 10516 (2009).
- [24] K. Zhao, Q. Zhang, M. Chini, Y. Wu, X. Wang, and Z. Chang, *Opt. Lett.* **37**, 3891 (2012).
- [25] A. T. Le, R. R. Lucchese, S. Tonzani, T. Morishita, and C. D. Lin, *Phys. Rev. A* **80**, 013401 (2009).
- [26] C. Jin, A. T. Le, and C. D. Lin, *Phys. Rev. A* **83**, 023411 (2011).
- [27] V. Tosa, H. T. Kim, I. J. Kim, and C. H. Nam, *Phys. Rev. A* **71**, 063807 (2005); **71**, 063808 (2005).
- [28] M. B. Gaarde, M. Murakami, and R. Kienberger, *Phys. Rev. A* **74**, 053401 (2006).
- [29] G. Tempea, M. Geissler, M. Schnürer, and T. Brabec, *Phys. Rev. Lett.* **84**, 4329 (2000).
- [30] T. Brabec and F. Krausz, *Rev. Mod. Phys.* **72**, 545 (2000).
- [31] C.-J. Lai and F. X. Kärtner, *Opt. Express* **19**, 22377 (2011).
- [32] X. M. Tong and C. D. Lin, *J. Phys. B* **38**, 2593 (2005).
- [33] C. Jin, A. T. Le, C. A. Trallero-Herrero, and C. D. Lin, *Phys. Rev. A* **84**, 043411 (2011).
- [34] P. Salières, P. Antoine, A. de Bohan, and M. Lewenstein, *Phys. Rev. Lett.* **81**, 5544 (1998).
- [35] Ph. Balcou, P. Salières, A. L'Huillier, and M. Lewenstein, *Phys. Rev. A* **55**, 3204 (1997).
- [36] M. B. Gaarde, J. L. Tate, and K. J. Schafer, *J. Phys. B* **41**, 132001 (2008).
- [37] C. Jin, G. J. Stein, K.-H. Hong, and C. D. Lin, *Phys. Rev. Lett.* **115**, 043901 (2015).
- [38] M. Geissler, G. Tempea, and T. Brabec, *Phys. Rev. A* **62**, 033817 (2000).
- [39] M. B. Gaarde and K. J. Schafer, *Phys. Rev. A* **65**, 031406 (2002).
- [40] A. Dubrouil, O. Hort, F. Catoire, D. Descamps, S. Petit, E. Eévil, V. V. Strelkov, and E. Constant, *Nat. Commun.* **5**, 4637 (2014).